Hindawi
Advances in Meteorology
Volume 2022, Article ID 7368882, 13 pages
https://doi.org/10.1155/2022/7368882

Research Article

Interannual Variations of Water and Carbon Dioxide Fluxes over a Semiarid Alpine Steppe on the Tibetan Plateau

Yang Liu,[1] **Huizhi Liu**,[1,2] **Fengquan Li**,[1,3] **Qun Du**,[1] **Lujun Xu**,[1] **and Yaohui Li**[4]

[1]*State Key Laboratory of Atmospheric Boundary Layer Physics and Atmospheric Chemistry, Chinese Academy of Sciences, Beijing 100029, China*
[2]*University of Chinese Academy of Sciences, Beijing, China*
[3]*Wuhan NARI Limited Liability Company of State Grid Electric Power Research Institute, Wuhan, China*
[4]*College of Aviation Meteorology, Civil Aviation Flight University of China, Guanghan, China*

Correspondence should be addressed to Huizhi Liu; huizhil@mail.iap.ac.cn

Received 28 December 2021; Revised 16 May 2022; Accepted 26 July 2022; Published 6 October 2022

Academic Editor: Maria Ángeles García

Water and carbon exchanges between grassland and the atmosphere are important processes for water balance and carbon balance. Based on eddy covariance observations over a semiarid alpine steppe ecosystem in Bange on the Tibetan Plateau during the growing season from 2014 to 2017, the variations in evapotranspiration (ET), net ecosystem exchange (NEE), and their components and the associated driving factors were analyzed. Linear and nonlinear models were applied to investigate the relationships between fluxes and their controlling factors over different timescales. The results show that the average ET for the growing season ranged from 1.1 to 2.4 mm/d with an average of 2.0 mm/d for the four consecutive years. Drought conditions reduced the surface conductance and hence the Priestley–Taylor coefficient. Mean T/ET was low (0.34) due to low vegetation cover. Plant growth increased the T/ET ratio during the growing season, whereas soil water content (SWC) explained most of the variation of ET and E on daily and monthly scales. The Enhanced Vegetation Index (EVI) was the most important controlling factor for temperature. Transpiration increased with SWC in dry conditions. For the growing season in 2014, 2016, and 2017, Bange was a carbon sink, while it was a carbon source in 2015. The largest CO_2 flux was higher and the temperature sensitivity coefficient (Q_{10}) was lower for 2015 than for the other three years. SWC affected these photosynthesis and respiration parameters. The ratio of respiration (Re) to gross primary production (GPP) was the highest during the 2015 growing season. Both on daily and monthly scales, Re was positively and linearly correlated with GPP. The most important controlling factor for the CO_2 flux was EVI on daily and monthly scales.

1. Introduction

Evapotranspiration (ET), which consists of transpiration (T) from the plant canopy and evaporation (E) from bare soil and leaf interception [1], is an important component of the terrestrial water balance and a link between carbon and energy cycles [2]. The ratio of T to ET (T/ET) represents the allocation between biological and physical processes for the ecosystem water flux [3]. Furthermore, the component fluxes of ET are used as the input, calibration, and validation of many hydrological and land surface models. The eddy covariance (EC) technique only provides observations of net ET fluxes. Partitioning ET into its component fluxes is important to interpret the water balance and ecological processes [4].

The CO_2 flux is affected by many environmental factors. Extreme climatic events (e.g., droughts) can lead to anomalies in carbon dioxide fluxes [5]. Both gross primary production (GPP) and ecosystem respiration (Re) can be affected by droughts and hence affect the magnitude of the net ecosystem exchange (NEE).

The Tibetan Plateau (TP) is the highest plateau in the world, with an average elevation of over 4000 m [6]. The Tibetan Plateau ecosystem is very sensitive to climate change [7]. From the beginning of this century, a lot of field experiments about the land-atmosphere interaction on the

Tibetan Plateau have been carried out [7–11]. Over an alpine meadow on the Qinghai-Tibetan Plateau, soil water content (SWC) and air temperature (Ta) were the most important environmental factors in surface energy partitioning on seasonal scales [12]. On the annual scale, the ratio of annual evapotranspiration (ET) to annual precipitation (PPT) is about 60% in the Haibei meadow [7] while the ratio nearly equals 1 for the alpine steppe in Shuanghu, Tibet, China [9]. The Tibetan Plateau spans nearly 29° of longitude and 15° of altitude. The water and CO_2 exchanges over grassland ecosystems vary in different climate zones. Information regarding ET and NEE is necessary to understand the responses of the Tibetan Plateau alpine steppe to climate change. Many studies on the Tibetan Plateau have been focused on the characteristics of ET. There is a need to partition ET over TP and examine how ET, NEE, and their components respond to the environmental and biological factors against the background of climate change.

In this context, eddy covariance measurements of water and carbon dioxide fluxes at the Bange site during the growing season (June to September) from 2014 to 2017 were used to analyze the variation of evapotranspiration and its components. The main objectives in this study were to (1) characterize the seasonal and interannual variations of ET and NEE and their partitioning over this semiarid alpine steppe; (2) determine the parameters of photosynthesis and respiration; and (3) investigate the important environmental and meteorological factors that control ET, NEE, and their components on daily and monthly scales.

2. Materials and Methods

2.1. Site Description. The observation site is located at Bange (31°25′N, 90°2′E elevation 4700 m) in a sub-frigid semiarid climatic zone on the Tibetan Plateau. This site is under the influence of the plateau monsoon, with a 30-year (1980–2010) mean annual air temperature of −2.8°C and an annual total precipitation of 308.3 mm, most of which falls from June to October. The soil is classified as light-color sandy loam. The land cover type of this site is alpine steppe, and the dominant species is *Stipa purpurea* (C3 grass), with a mean plant height of less than 3 cm throughout the growing season. In this study the growing season is defined as the period from June to September.

2.2. EC Measurements and EVI. Based on the "Third Tibetan Plateau Scientific Experiment," the site was set up on 15 July 2014 with measurements taken until 6 September 2017. Water vapor and carbon dioxide concentrations were measured using the EC system, which consisted of a three-dimensional sonic anemometer (CSAT-3, Campbell, USA) and an open-path CO_2/H_2O infrared gas analyzer (LI-7500A, LI-COR, USA). Continuous auxiliary measurements of meteorological and environmental conditions were also performed (Table 1). More details of this site and measurements are described in Wang et al. [8].

As a proxy for grass phenology, the Enhanced Vegetation Index (EVI) with a spatial and temporal resolution of 250 m and 16 days, respectively, was retrieved from the Moderate-Resolution Imaging Spectroradiometer (MODIS, MOD13Q1). To transform biweekly EVI data into daily intervals, the data were linearly interpolated to fill gaps.

Table 1: Variables, instruments, and measurement heights.

Variables	Instruments	Measurement heights [m]
Temperature	HMP45C, Campbell	2, 4, 10
Relative humidity	HMP45C, Campbell	2, 4, 10
Wind speed	010C, Campbell	2, 4, 10
Wind direction	020C, Campbell	10
Net radiation	CNR4, Kipp & Zonen	1.5
PAR	LI190SB, LI-COR	1.5
Soil heat flux	HFP01, Hukseflux	0.05, 0.1 (depth)
Soil temperature	109-L, Campbell	0.05, 0.1, 0.2, 0.5, 1 (depth)
Soil water content	CS616, Campbell	0.05, 0.1, 0.2, 0.5, 1 (depth)
Precipitation	52202, Young	—

2.3. Flux Calculation and Post-processing. The EddyPro 6.2.0 package was used to process the 10 Hz raw data and calculate 30 min-averaged fluxes. Post-processing of the raw data mainly included double rotation [13] for tilt correction, spectral loss correction [14], and WPL density fluctuation correction [15].

In addition, the test of the stationary conditions for LE and the integral turbulence characteristics was performed as described by [16]. To produce a continuous dataset, data gaps were filled with look-up tables and mean diurnal course methods.

2.4. Partitioning of ET and Treatments of NEE. The ET partitioning method employed in this study, known as FVS method, is based on the analysis of the correlation structure of CO_2 and H_2O. It assumes that the flux variance similarity theory applies separately to CO_2 and H_2O stomatal (photosynthesis, transpiration) and non-stomatal (respiration, evaporation) components. Using the estimated leaf-level water use efficiency (WUE) as input, the FVS method calculates the contribution of each component to the total fluxes of ET, and thus the magnitude of each component flux can be determined. WUE is the only input parameter needed in the FVS method. WUE was estimated as follows:

$$\mathrm{WUE} = 0.7\frac{\overline{c_s} - \overline{c_i}}{\overline{q_s} - \overline{q_i}} = 0.7\frac{\overline{c_s}(1-k)}{\overline{q_s} - \overline{q_i}}, \quad (1)$$

where c_s and q_s are the concentrations of carbon dioxide and water vapor at the leaf surface, respectively, which were inferred from the EC-measurement level value by considering the mean profile; c_i and q_i represent the inter-stomatal concentrations of carbon dioxide and water vapor, respectively. q_i was assumed to be saturated at the leaf surface temperature (estimated as air temperature), and c_i was calculated from $\overline{c_s}$ by parameterizing the $\overline{c_i}/\overline{c_s}$ ratio, k [17]. For C_3 species, k was parameterized as follows:

$$k = -0.084\left(\overline{q_i} - \overline{q_s}\right) + 0.8793. \quad (2)$$

The partitioning of ET fluxes was applied to half-hourly measurements during the daytime.

The van't Hoff equation was applied to partition NEE into Re and GPP [18]. Specifically, the nighttime half-hourly NEE data (assumed to be equal to nighttime Re) were fitted against the soil temperature at a depth of 5 cm (Ts) using the following formula:

$$R_e = ae^{bT_s}, \tag{3}$$

where a and b are the regression parameters. Then, the daytime estimates of R_e were derived using daytime T_s and (3). GPP was calculated as the difference between NEE and Re:

$$\mathrm{GPP} = R_e - \mathrm{NEE}. \tag{4}$$

The Michaelis–Menten model was used to describe the relationship between daytime NEE (F_c) and PAR:

$$F_c = \frac{F_{\max}\alpha \mathrm{PAR}}{F_{\max} + \alpha \mathrm{PAR}} + \mathrm{Re}_{\mathrm{bulk}}, \tag{5}$$

where PAR is the photosynthetic active radiation (μmol m^{-2}s^{-1}), $F_{\max}$ is the NEE at a saturating light level (μmol m^{-2}s^{-1}), α is the apparent quantum yield (μ mol CO_2 μ mol^{-1} photons), and $\mathrm{Re}_{\mathrm{bulk}}$ is the bulk estimated Re.

2.5. Calculation of Bulk Surface Parameters. The bulk parameter of surface conductance (G_s) was employed to represent the surface-atmosphere exchange efficiency [19]. By inverting the Penman–Monteith equation, G_s (ms^{-1}) was derived as follows [20]:

$$G_s = \frac{G_a \gamma \mathrm{LE}}{\rho_a C_p G_a VP\ D + \Delta H - \gamma \mathrm{LE}}, \tag{6}$$

where G_a is the aerodynamic conductance (ms^{-1}), and $G_a = (1/(u/u_*^2) + 6.2u_*^{-0.67})$ in which u is the wind speed (ms^{-1}); γ is the psychrometric constant (kPa K^{-1}); ρ_a is the air density (kg m^{-3}); C_p is the specific heat of air at constant pressure (J kg^{-1} K^{-1}); VPD is the vapor pressure deficit (kPa); Δ is the slope of the vapor pressure curve at the mean air temperature (kPa K^{-1}); and H is the sensible heat flux (W m^{-2}).

The Priestley–Taylor coefficient α was calculated as the ratio of the actual evapotranspiration rate (ET) to the equilibrium evapotranspiration rate ($\mathrm{ET}_{\mathrm{eq}}$):

$$\alpha = \frac{\mathrm{ET}}{\mathrm{ET}_{\mathrm{eq}}} = \frac{\Delta + \gamma}{\Delta} \frac{\mathrm{LE}}{R_n - G}, \tag{7}$$

where R_n is the net radiation (W m^{-2}) and G is the soil heat flux (W m^{-2}).

3. Results

3.1. Meteorological Conditions. The daytime average downward solar radiation (Rs) ranged from 205.7 to 689.3 wm^{-2}, with a mean value of 464.9 wm^{-2} (Figure 1(a)). The air temperature (Ta) and soil temperature at 5 cm depth (Ts) corresponded well with Rs. Following the variability of Rs, Ta and Ts increased at the beginning of the growing season, peaked in mid-growing season, and then decreased (Figure 1(b)). The daytime-mean Ta and Ts were generally higher than 5°C except at the end of the 2014 growing season. During the growing season of 2016, Ta was lower than that in 2015 or 2017 (Table 2). The lower temperature in the early growing season may have caused the delayed onset of the plant green-up day.

The daytime-mean wind speed (WS) at Bange was about 4 m/s during the growing season. WS in 2014 was clearly lower than that during the other three years (Figure 1(c)). During the growing season in 2015, the vapor pressure deficit (VPD) was the largest (Figure 1(d)), and the soil water content at 5 cm depth (SWC) was the lowest (Figure 1(e)). The fluctuations of VPD and SWC were mainly affected by the precipitation. Bange received the lowest amount of precipitation in 2015, indicating that severe drought and water deficit may have limited ET and its component fluxes that year.

The timing when EVI reached its peak value was different for each year (Figure 2). EVI peaked in late August, early September, late August, and late July from 2014 to 2017, respectively (Figure 2). The mean value of EVI during the growing season for the consecutive four years was 0.21, 0.13, 0.17, and 0.20, respectively. Although the steppe received more precipitation in June 2016 than in June 2017, the lower temperature may have hindered plant growth, and thus EVI in 2016 was lower.

3.2. Variations of ET, $\mathbf{G_s}$, and ET/ET_{eq}. The temporal variation pattern of ET was highly related to the variations of Rs and SWC. The intra-seasonal trends of ET in 2014 and 2017 were not significant due to the even distributions of precipitation. By contrast, the inter-seasonal trend of ET in 2015 and 2016 was obvious due to the uneven distribution of precipitation (Figure 3(a)). ET in 2015 showed clear seasonal variation corresponding to rainfall events, which recharged the soil water during this drought year. ET in 2016 peaked in July. The average ET values were 2.2 mm/d and 1.1 mm/d for the growing season in 2014 and 2015, respectively, while the mean values of ET were larger for 2016 and 2017 with a value of 2.4 mm/d for both years. The mean ET value for the whole study period was 2.0 mm/d, and the maximum daily ET was 3.9 mm/d, which occurred both in 2016 and 2017. This is consistent with the mean daily ET over another alpine steppe at 4947 m a.s.l. [9] with a mean value of 2.1 mm/d and a maxima of 4.2 mm/d.

The variation of daily G_s corresponded well with that of ET (Figure 3(b)). G_s increased gradually, peaked during the mid-growing season, and then decreased. The variation pattern of G_s was clearly modified by the precipitation events. It was less than 10.0 mm s^{-1} when no precipitation occurred, whereas G_s reached a relatively high value following precipitation, particularly in 2016 and 2017. The mean value of G_s at this site was 10.0 mm s^{-1} ($\pm$ 7.0 mm s^{-1}) and the maxima was 32.6 mm s^{-1}, which occurred in 2017.

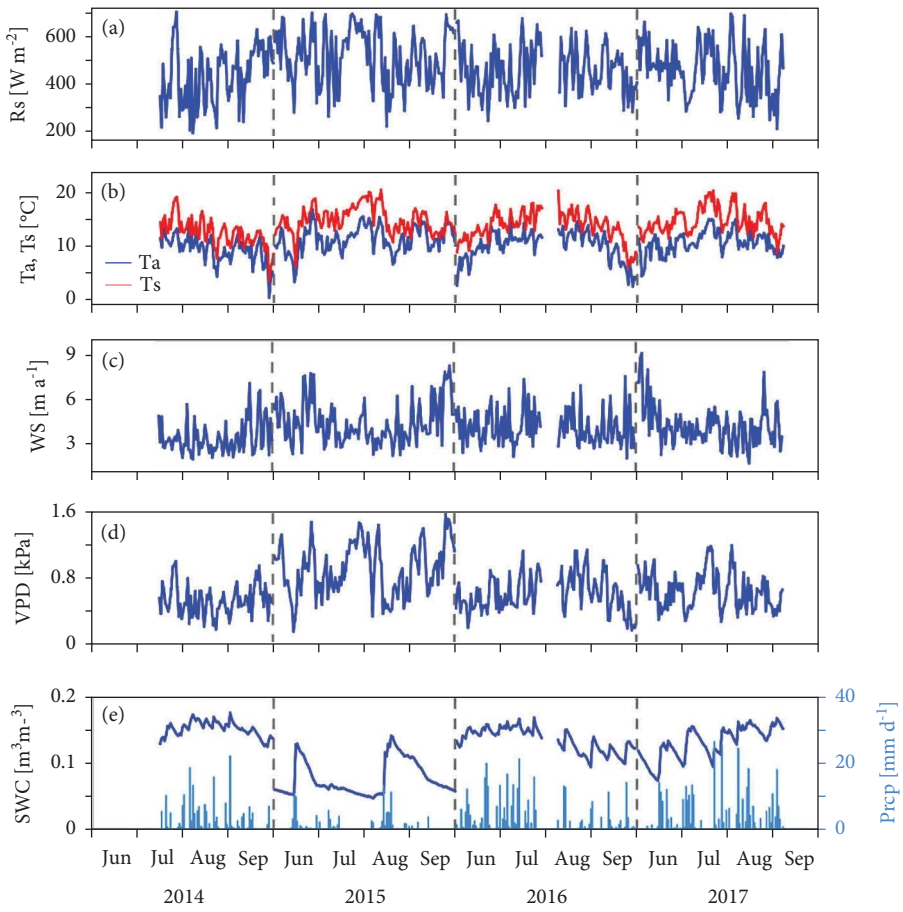

Figure 1: Seasonal variations of daytime average downward solar radiation (Rs), air temperature (Ta), wind speed (WS), vapor pressure deficit (VPD), precipitation, and soil water content at 5 cm depth below ground (SWC) during the growing season from 2014 to 2017. The daytime average of the variable was calculated with half-hourly data at conditions of $Rs > 100\ wm^{-2}$.

Table 2: Periodical average of the daytime-mean shortwave radiation (Rs), air temperature (Ta), soil temperature at 5 cm depth (Ts), vapor pressure deficit (VPD), wind speed (WS), soil water content at 5 cm depth (SWC), and periodical sum of precipitation (PPT) for the growing season from 2014 to 2017.

	Rs [$W\ m^{-2}$]	Ta [°C]	Ts [°C]	WS [ms^{-1}]	VPD [kPa]	SWC [$m^3\ m^{-3}$]	PPT [mm]
2014	218.7	9.4	12.5	3.37	0.53	0.15	209.6
2015	278.1	11.5	15.1	4.40	0.91	0.08	121.3
2016	240.6	10.1	13.8	4.15	0.61	0.13	392.1
2017	247.2	10.8	14.9	4.21	0.64	0.13	373.5

The mean value of G_s during the growing season was lower than that of alpine meadows on the Qinghai-Tibetan Plateau (11.0 $mm\ s^{-1}$ [12]), but it was greater than that of another semiarid alpine steppe on TP (7.5 $mm\ s^{-1}$, [9]).

The Priestley–Taylor coefficient α (=ET/ET_{eq}) was significantly lower than the suggested value of 1.26 for humid climates (Figure 3(c)), indicating that the surface was far from saturated. The α ranged between 0.09 and 1.02 with a mean value of 0.47 for the whole study period. The averageα during the growing season for the four consecutive years was 0.61, 0.31, 0.50, and 0.51, respectively. The small magnitude of α in 2015 represents the limitation of the water supply contributing to the low ET, which may also be reflected in the magnitude of SWC. Therefore, the low ET rate for the growing season in 2015 was attributed to the water deficit rather than the low atmospheric evaporative demand or available energy. Zhang et al. [21] measured a value of α in the growing season at Haibei over QTP of 1.37, which is higher than 1.26, and they concluded that net radiation limits ET over the alpine meadow.

3.3. Variation of ET Partitioning. The variation of direct evaporation (E) and plant transpiration (T) is shown in Figure 4(a). E was overall much greater than plant T, except during dry conditions. The mean E for each growing season was 1.55, 0.78, 1.59, and 1.43 mm/d, respectively, from 2014 to 2017 with an ensemble mean of 1.33 mm/d (Table 3). As for T,

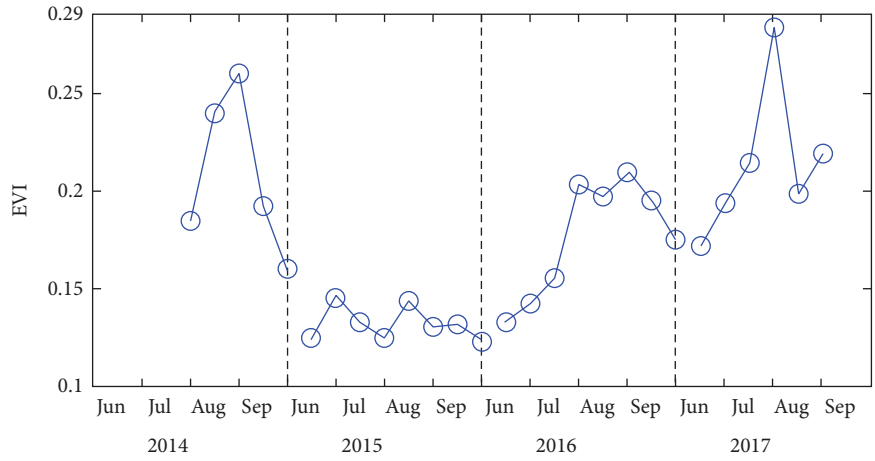

Figure 2: Variations of EVI during the growing season from 2014 to 2017.

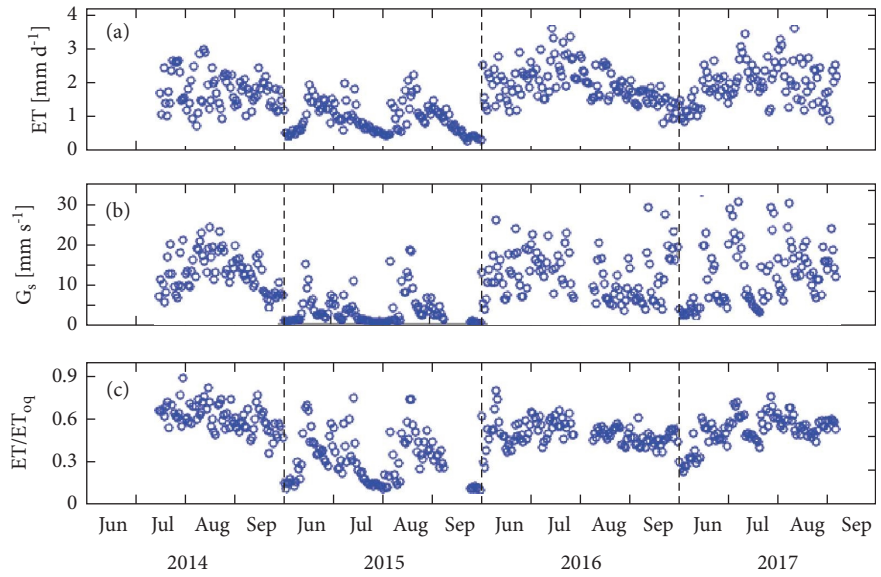

Figure 3: Variations of ET, G_s, and ET/ET$_{eq}$ throughout the growing season from 2014 to 2017.

the mean value was 0.62, 0.43, 0.73, and 0.94 mm/d for the four years, respectively, with an ensemble mean of 0.68 mm/d.

The ratio of transpiration to evapotranspiration (T/ET) ranged from 0.03 to 0.84 throughout the measurement period, with a mean value of 0.34 (Figure 4(b)). For each year, mean T/ET was 0.29, 0.36, 0.31, and 0.40, respectively. Compared with other grasslands over QTP, the Bange site had a much lower T/ET. The maximum T/ET for 2016 was 0.72 when EVI reached its peak. Hu et al. [22] reported a maximum T/ET value of ca. 0.8 during conditions of peak LAI at an alpine shrub-meadow. Similarly [23], reported a maximum T/ET that reached 0.93–0.98 (mean = 0.96) over alpine grassland during the peak growing season. Our result is consistent with previous studies and shows that the contribution of evaporation to ET reduced with plant growth. However, the maximum T/ET was significantly lower than 1 due to the low vegetation cover at this site.

The seasonal pattern of T/ET was related to plant growth but strongly modified by SWC (Figure 5). During drought conditions in 2015, the maximum T/ET reached 0.84, which is greater than the maximum value of 2016 (0.72). Fewer rainfall events resulted in less wetting of the surface for evaporation, which therefore reduced E, whereas grass could use available root-zone soil water for transpiration, which was less available for E [24]. This effect of SWC on T/ET has been previously reported over different ecosystems including desert shrubland, savanna, and a grassland site in Arizona, USA [25].

3.4. Variations of NEE, GPP, and Re. The seasonal and interannual variation of daily gap-filled and partitioned NEE, GPP, and Re are displayed in Figure 6 and Table 4. For substantial parts of the wet years (2014, 2016, and 2017), the steppe ecosystem was a net sink of CO_2 characterized by the negative value of NEE. However, for late June and August in 2015 and for the early growing season in June 2016, this ecosystem was a strong source of CO_2, and NEE reached a maximum of 1.25 g C m^{-2}d^{-2} on 14 August 2015.

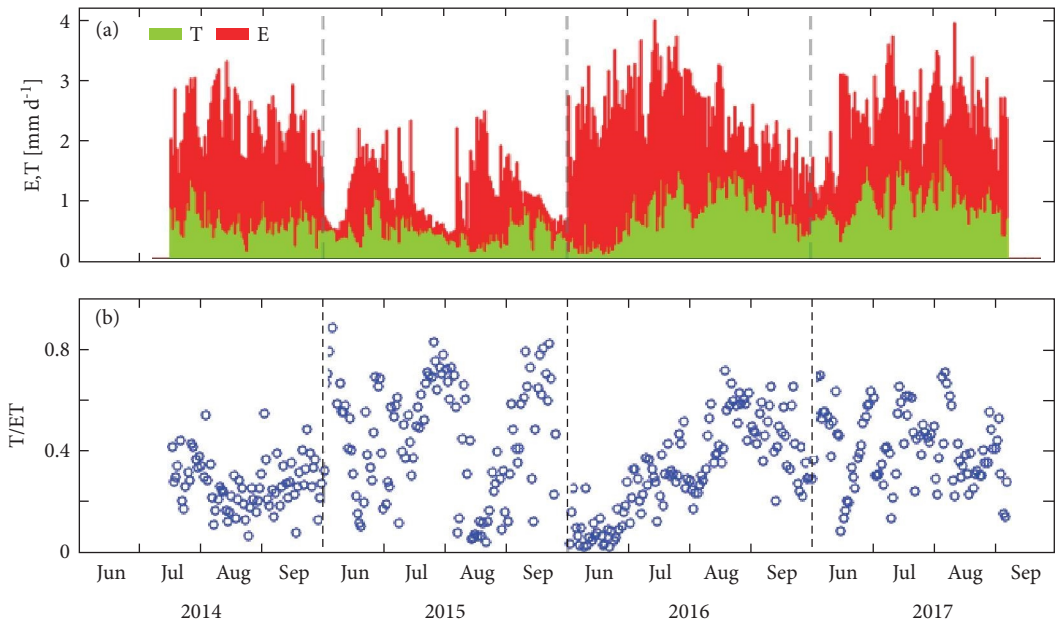

Figure 4: Variations of mean daily ET (mm/d), E (mm/d), T (mm/d), and T/ET for the growing season from 2014 to 2017.

Table 3: Mean ET, *E*, *T*, and T/ET for the growing season from 2014 to 2017 (mm/d).

Year	ET	E	T	T/ET
2014	2.17	1.55	0.62	0.29
2015	1.21	0.78	0.43	0.36
2016	2.32	1.59	0.73	0.31
2017	2.37	1.43	0.94	0.40

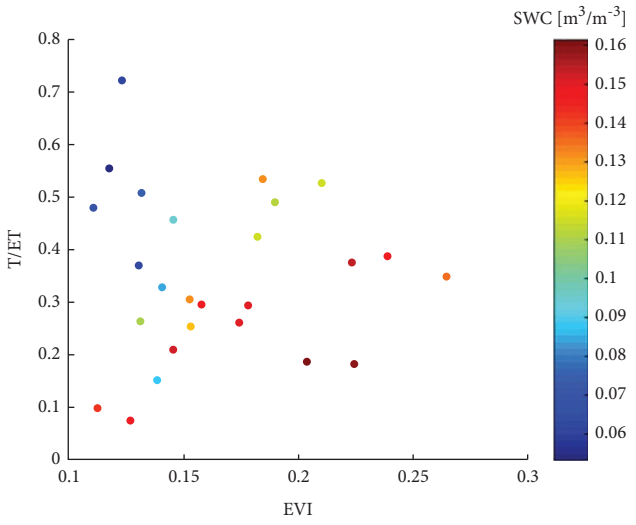

Figure 5: The relationship between 16 d averaged T/ET and MODIS EVI. The color shading represents the value of SWC. The gray ellipse highlights the extremely dry conditions during 2015. The gray rectangle indicates wet conditions.

The maximum daily GPP during the growing season was 2.00, 0.70, 1.97, and 2.24 g C m^{-2}d^{-2} for the four years, respectively. The GPP in the drought year of 2015 was clearly lower than that during the other three years, consistent with the lower EVI. During this drought year, Re was also lower than that for the wet years.

4. Discussion

4.1. Biological Control of ET via Surface Conductance. The surface conductance G_s (mm s^{-1}) is the total conductance representing the aggregation of plant transpiration, plant interception evaporation, and bare soil evaporation [26]. The relationship between G_s and environmental factors is investigated in this section. G_s was responsive to available water but insensitive to air temperature and radiation (data not shown). Specifically, G_s decreased with increasing VPD (Figure 7(a)). The G_s-VPD relationship is expressed with an exponential model:

$$G_s = 34.62 \exp(-1.90\,\mathrm{VPD}), \quad R^2 = 0.51, \tag{8}$$

indicating that when VPD was at a low level (less than about 0.7 kPa), a minor increase of VPD caused a substantial decrease in G_s. However, as VPD continued to increase and exceeded a critical value of ca. 1.2 kPa, the magnitude of G_s almost became insensitive to the variation of VPD and stabilized at a constant small value. Similar results have been reported in other grassland ecosystems over TP (e.g., [18, 20]) and North America (e.g., [27]), forest ecosystems (e.g., [28, 29]), and desert shrub (e.g., [30]). Since the

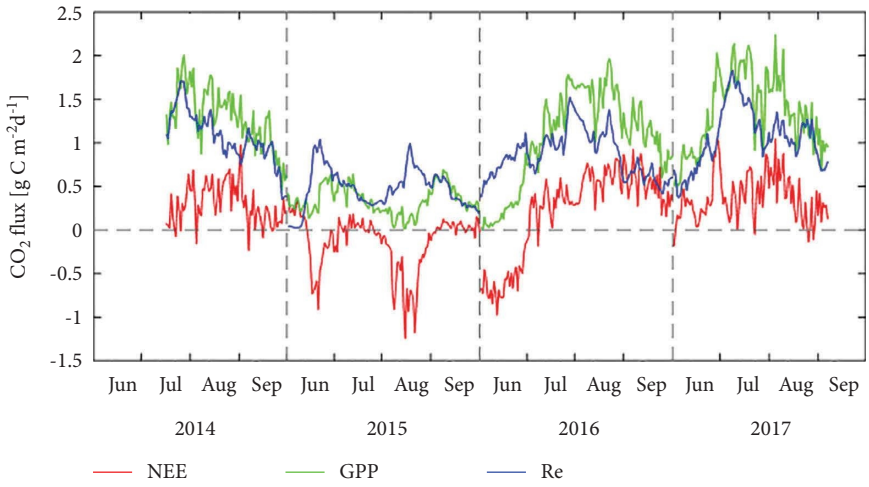

Figure 6: Variations of NEE, Re, and GPP throughout the growing season from 2014 to 2017.

Table 4: Total NEE, Re, and GPP for the growing season from 2014 to 2017 (gC $m^{-2}mon^{-1}$).

Year	NEE	Re	GPP	Re/GPP
2014	−17.77	85.13	102.90	0.83
2015	16.83	60.02	43.19	1.39
2016	−21.96	108.89	130.85	0.83
2017	−29.39	107.65	137.04	0.79

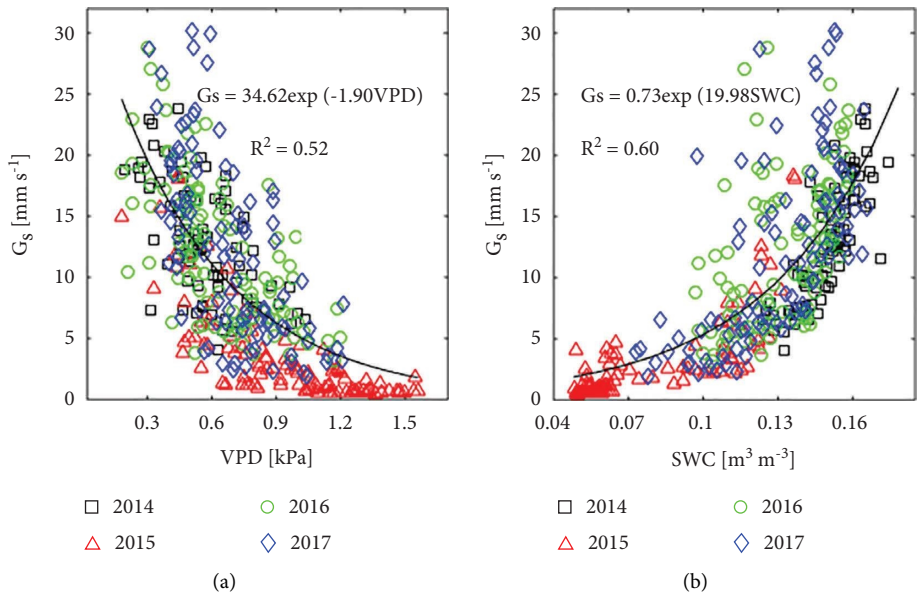

Figure 7: Variations of G_s with VPD (a) and SWC (b).

magnitude of SWC was highly negatively correlated with that of VPD (data not shown), G_s was also controlled by SWC, and the G_s-SWC relationship was more significant than the G_s-VPD one (Figure 7(b)):

$$G_s = 0.73 \exp(19.98\,\mathrm{SWC}), \quad R^2 = 0.60. \tag{9}$$

This relationship was consistent with that found in the low range of SWC in a semiarid steppe over Inner Mongolia [31]. However, an expected capping of G_s as the SWC exceeded a critical value (0.16 m^3m^{-3} reported by [8]) was not observed in this study. G_s is expected to remain constant as the SWC continues to increase. However, a positive linear relationship between G_s and SWC was reported at another

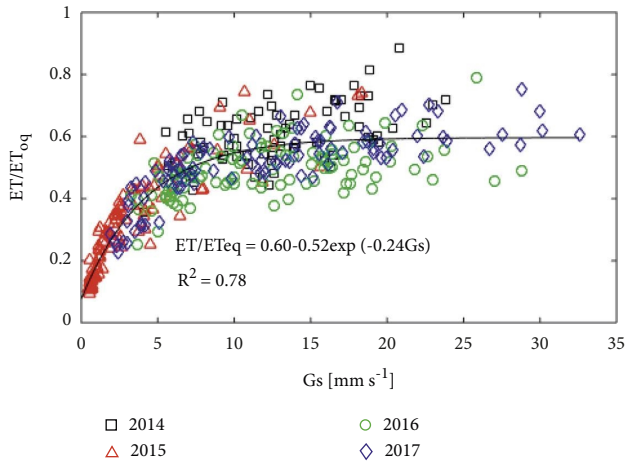

FIGURE 8: Relationship between the daily average surface conductance (G_s) and the Priestley–Taylor coefficient (α = ET/ET_{eq}).

alpine meadow on the Qinghai-Tibetan Plateau [26] with SWC ranging between ~0.05 and 0.35 m^3m^{-3}. It is expected that G_s will reach a maximum value and then stabilize. The critical value of SWC above which G_s stabilizes for the QTP region remains to be further investigated.

G_s represents the combined effect of VPD, Rn, SWC, and physiological rhythm of plants [23]. The relationship between G_s and α (ET/ ET_{eq}) reflects the interactive effects of SWC and LAI with the photosynthesis capacity [32, 33, 34]. Therefore, although individual factors (e.g., precipitation and SWC) varied considerably throughout the study period, ET/ ET_{eq} was scaled with G_s as follows:

$$\frac{ET}{ET_{eq}} = 0.60 - 0.52\ \exp\left(-0.24G_s\right), \quad R^2 = 0.78. \tag{10}$$

In 2015 G_s was relatively small and the G_s-α relationship fitted (8) well, while in 2016 and 2017 when G_s was relatively large, the G_s-α plot displays some scatter to the fitted line (Figure 8). The magnitude of α increased with G_s in a low G_s section (less than about 12 mm s^{-1}), but when G_s exceeded this threshold, α became less sensitive to G_s. This threshold was consistent with the theoretical value (16 mm s^{-1}, [35]) and values from other alpine steppes (e.g., 13 mm s^{-1}, [9]; 15 mm s^{-1}, [36]).

4.2. Environmental and Meteorological Controls of Water Flux. To better characterize the variation of ET and its components, the relationships between E and T and environmental (SWC) and meteorological (Ta and VPD) factors were investigated on the daily scale. Rn was not a major factor (data not shown) indicating that the exchange of water fluxes was not energy-limited at Bange, different from that of a humid alpine meadow [21].

E and T responded to SWC differently (Figure 9). Precipitation at this site has large seasonal variation, which can influence the recharge of soil water. Furthermore, during some periods of the study, there was a shortage of soil water. When SWC was lower than about 0.1 m^3m^{-3}, both E and T increased with SWC. As SWC continued to increase, E also kept increasing, whereas T became less sensitive to SWC and fluctuated around 0.8 mm d^{-1}, indicating that the optimal SWC for plant transpiration was greater than about 0.1 m^3m^{-3}.

Because T became insensitive to the variation of SWC, when SWC reached a critical value, the relationship between T and meteorological factors was analyzed to better understand the variation of T under wet conditions. Only data with SWC > 0.1 m^3m^{-3} were used for the analysis. Significant linear T-Ta and T-VPD relationship were observed (Figure 10). At high SWC levels, the increase of both Ta and VPD caused an increase of T.

On the monthly scale, both ET and E were linearly and positively correlated with SWC (Figure 11(a) and 11(b)). SWC alone explains 73% (78%) of the variation in ET (E), indicating that water availability was the main factor controlling the long-term ET and E. At the monthly scale, no single factor explained the variation of T. Multiple factors were closely related to plant growth rather than the environmental or meteorological variables. Such a positive linear relationship between T and EVI is consistent with previous work at other grassland sites (e.g., [27]). However, some scatter exists in the T-EVI fit due to the influence of VPD, which represents the evaporative demand.

4.3. The Relationship between Daytime NEE and PAR under Different SWC. The relationship between the daytime half-hourly NEE and PAR was described with the Michaelis–Menten model. The NEE-PAR relationships showed a similar pattern for 2014, 2016, and 2017 (Figure 12(a)). For these three years, the NEE reached its minimum at PAR of 1300 μ mol $m^{-2}s^{-1}$. When PAR was less than 1300 μ mol $m^{-2}s^{-1}$, the daytime NEE decreased with the increasing PAR. For PAR greater than 1300 μ mol $m^{-2}s^{-1}$, the daytime NEE increased with PAR. F_{max} ranged from −3.97 to −4.65 μ mol $m^{-2}s^{-1}$ (Table 5). By contrast, the relationship was significantly different for 2015 compared with the other three years. During 2015, the PAR critical value reduced to 600 μ mol $m^{-2}s^{-1}$, and F_{max} decreased to −0.99 μ mol $m^{-2}s^{-1}$.

To further investigate the influence of SWC on the NEE-PAR curve, the NEE-PAR curves classified by wet (SWC > 0.1 m^3m^{-3}) and dry (SWC <= 0.1 m^3m^{-3}) conditions are displayed in Figure 12(b). For the purpose of reducing measurement errors [36, 37], the daytime NEE was further subdivided and then averaged based on each PAR level (100 μ mol $m^{-2}s^{-1}$ per PAR bin) under different conditions of SWC. The results show that α increased, but F_{max} decreased under dry conditions (Table 5).

4.4. The Relationship between Nighttime NEE and $\mathbf{T_s}$. The nighttime NEE increased exponentially with increasing T_s, and the Q_{10} during the growing season ranged from 1.16 to 1.98 from 2014 to 2017 with the minimum value of Q_{10} in 2015. These values were in the normal but lower range of previous studies [36]. The magnitudes of Q_{10} were

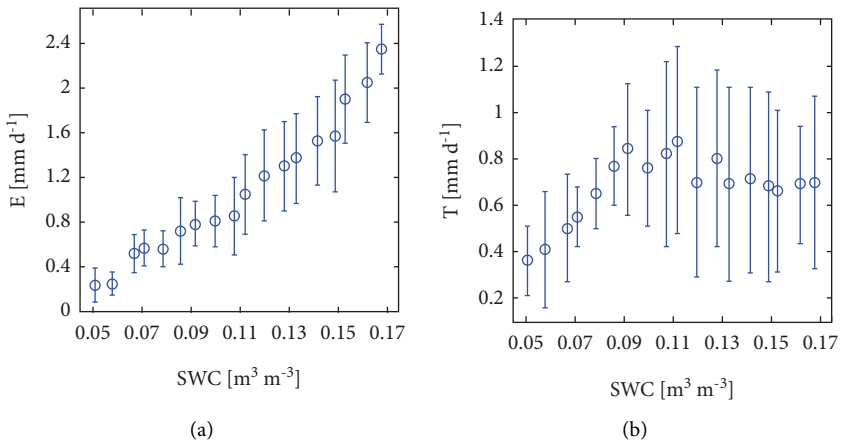

Figure 9: Relationship of E (a) and T (b) with SWC.

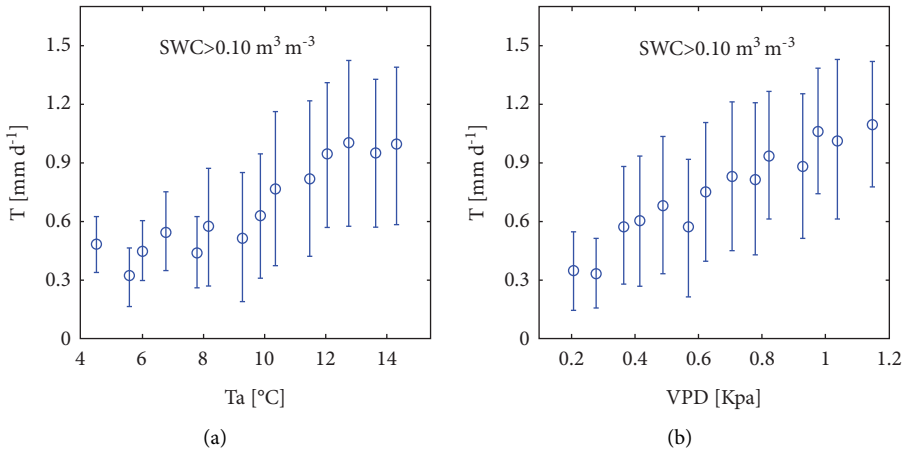

Figure 10: Variations of daily mean T against Ta (a) and VPD (b) at conditions of SWC greater than 0.1 m^3m^{-3}.

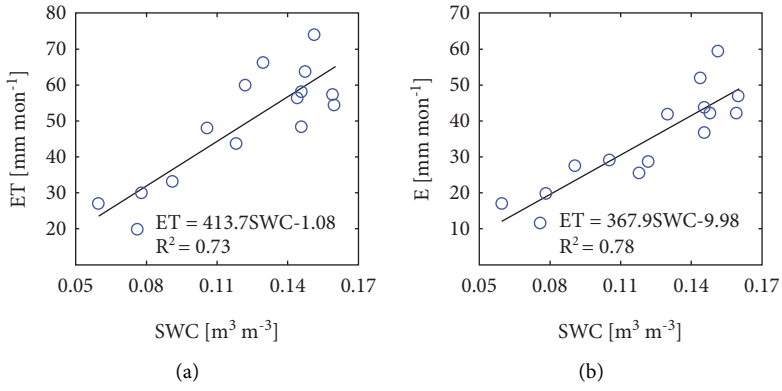

Figure 11: Relationship of the monthly total ET (a) and E (b) with SWC.

significantly lower than those for QTP pasture (3.0, [37]). During dry conditions, the Q_{10} value was lower than that during wet conditions (Table 6, Figure 13).

4.5. The Relationship between Re and GPP with Different EVI. Re was positively correlated with GPP on both daily and monthly scales (Figure 14). There was some scatter from the fitted Re-GPP line, as shown in the gray ellipse, indicating that Re was much greater than GPP. This phenomenon mainly occurred in 2015 and June 2016 when EVI was low. The ratio of total Re to total GPP (Re/GPP) during the growing season was 0.83, 1.39, 0.83, and 0.79 for the four consecutive years, respectively. A ratio of Re/GPP less than 1 indicates that NEE was negative. For the growing season of

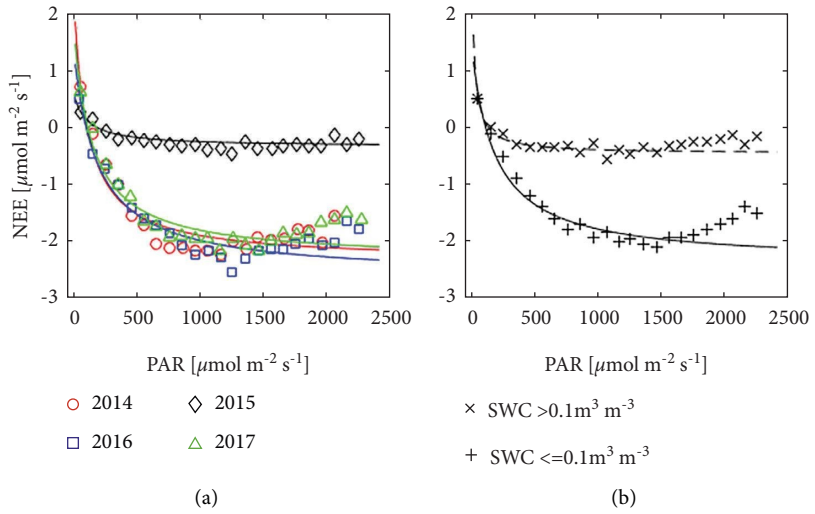

Figure 12: Relationship between the daytime half-hourly NEE and PAR for the growing season from 2014 to 2017 (a), and the whole dataset classified by SWC (b). The NEE and PAR data were averaged using PAR bins of 100 μ mol $m^{-2}s^{-1}$.

Table 5: The ecosystem photosynthesis parameters that describe the daytime NEE-PAR relationship using the Michaelis–Menten model.

Treatment	SWC	F_{max}	α	Re_{bulk}	R^2
2014	0.150	−4.65	−0.043	2.31	0.89
2015	0.076	−0.99	−0.009	0.63	0.78
2016	0.133	−3.97	−0.021	1.36	0.93
2017	0.130	−4.10	−0.028	1.78	0.92
SWC > 0.1		−3.75	−0.024	1.52	0.90
SWC < 0.1		−1.10	−0.046	1.45	0.72

Table 6: Parameters describing the relationship between nighttime NEE and T_s using (3) and (4).

Treatment	SWC	a	b	R^2	Q_{10}
2014	0.150	0.483	0.054	0.88	1.72
2015	0.076	0.319	0.015	0.50	1.16
2016	0.133	0.323	0.068	0.94	1.98
2017	0.130	0.402	0.062	0.98	1.86
SWC > 0.1		0.374	0.065	0.96	1.92
SWC < 0.1		0.219	0.029	0.57	1.34

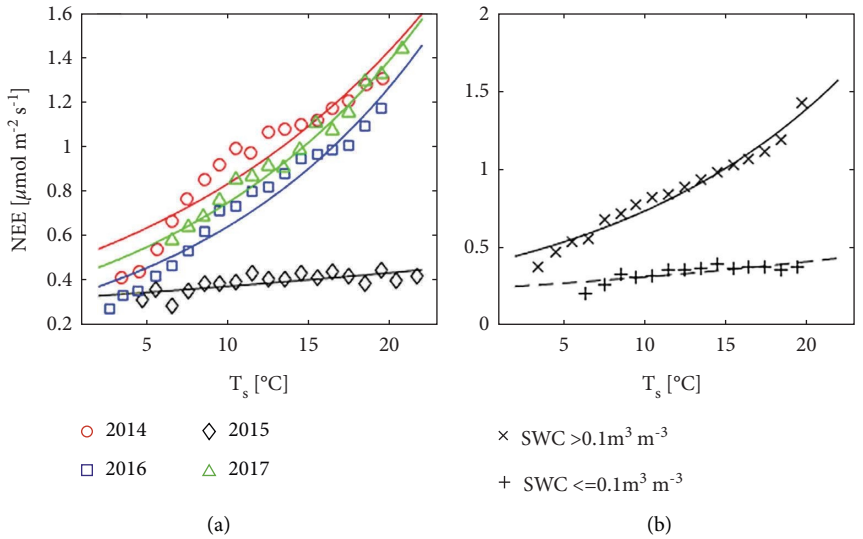

Figure 13: Relationship between nighttime half-hourly NEE and T_s for the growing season from 2014 to 2017 (a), and the whole dataset classified by SWC (b). The nighttime NEE data were averaged using T_s bins of 1°C.

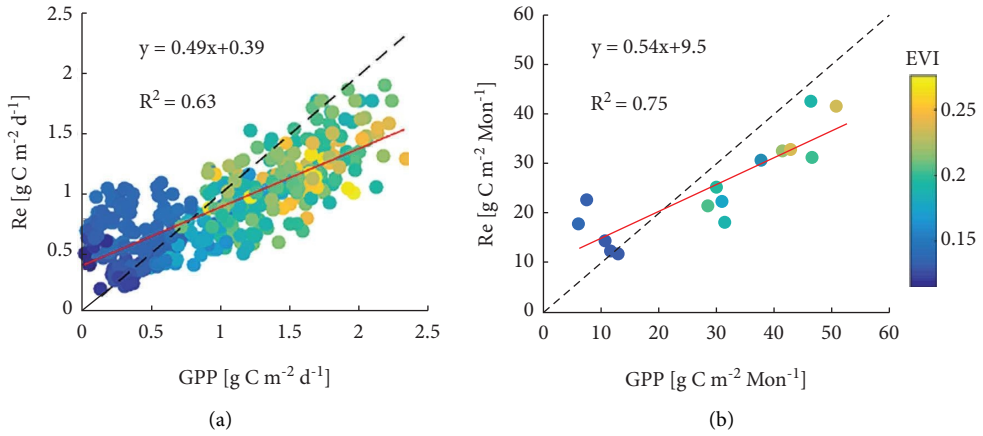

Figure 14: Relationship between daily (a) and monthly (b) Re and GPP during the growing season from 2014 to 2017. Color shading represents EVI values.

Table 7: Multiple stepwise linear regression analysis showing the optimum model variables, their parameters, and relative importance on daily and monthly timescales for the water (ET, *E*, and *T*) and carbon (NEE, Re, and GPP) fluxes.

Flux (y)	Timescale	R^2	Optimum model*	Relative importance of the parameters (scaled to 1)
ET (mm/d)	Day	0.71	$y = -1.963 + 11.409$ SWC $+ 0.004$ Rn $+ 0.094$ Ts $- 0.542$ VPD	SWC = 0.50; Rn = 0.29; Ts = 0.12; VPD = 0.10
	Month	0.91	$y = -3.657 + 13.285$ SWC $+ 0.095$ Ts $+ 0.007$ Rn	SWC = 0.64; Rn = 0.30; Ts = 0.06
E (mm/d)	Day	0.66	$y = -1.471 + 8.549$ SWC $+ 0.005$ Rn $- 0.84$ VPD $+ 0.05$ Ts	SWC = 0.47; Rn = 0.32; VPD = 0.17; Ts = 0.05
	Month	0.77	$y = -0.32 + 11.978$ SWC	SWC = 1.00
T (mm/d)	Day	0.51	$y = -0.767 + 5.474$ EVI $+ 0.407$ VPD	EVI = 0.84; VPD = 0.16
	Month	0.70	$y = -2.023 + 6.008$ EVI $+ 0.183$ WS $+ 0.049$ Ts	EVI = 0.72; Ts = 0.15; WS = 0.13
NEE (gC $m^{-2}s^{-1}$)	Day	0.50	$y = 0.922 - 8.980$ EVI $+ 2.008$ SWC $+ 0.002$ Rn $- 0.001$ PAR	EVI = 0.85; SWC = 0.07; Rn = 0.05; PAR = 0.03
	Month	0.56	$y = 1.076 - 6.927$ EVI	EVI = 1
Re (gC $m^{-2}s^{-1}$)	Day	0.72	$y = -1.018 + 2.381$ EVI $+ 6.039$ SWC $+ 0.064$ Ts	SWC = 0.46; EVI = 0.38; Ts = 0.16
	Month	0.54	$y = -0.339 + 6.767$ EVI	EVI = 1
GPP (gC $m^{-2}s^{-1}$)	Day	0.76	$y = -1.896 + 10.327$ EVI $+ 0.053$ Ts $+ 4.768$ SWC $- 0.003$ Rn $+ 0.612$ PAR	EVI = 0.65; SWC = 0.21; Ts = 0.08; Rn = 0.02; PAR = 0.04
	Month	0.79	$y = -1.275 + 12.721$ EVI	EVI = 1

*Units: SWC (m^3 m^{-3}); Rn (W m^{-2}); T_s (°C); VPD (kPa); EVI (–); PAR (μ mol $m^{-2}s^{-1}$).

2014, 2016, and 2017, this semiarid steppe acted as a carbon sink, while it was a carbon source in 2015.

4.6. Modeling the Relationships between the Observed Variables. On the daily scale, multiple stepwise linear regression analysis indicated that both ET and *E* could be modeled by the combination of four environmental variables, namely, SWC, Rn, Ts, and VPD. According to relaimpo analysis, SWC was the most important factor in these four variables followed by Rn (Table 7). On the monthly scale, ET variability is mainly explained by three variables, namely, SWC, Rn, and Ts, while *E* is explained by SWC. EVI was not significantly related to ET or *E*. By contrast, the most important variable to explain the variability of *T* was EVI on both daily and monthly scales. Because *T* is a stomatal component whereas *E* is a nonstomatal component, the EVI control on *T* was greater than that on *E*.

The multiple linear model indicates that on both daily and monthly scales, the most important predictor of the carbon flux is EVI. Specifically, on the monthly scale, EVI alone explains 56%, 54%, and 79% of the variability of NEE, Re, and GPP, respectively.

5. Conclusion

With four consecutive years of eddy covariance observations of water and carbon dioxide fluxes over an alpine steppe on the Tibetan Plateau, the interannual variations of ET, NEE, and their components were investigated. Using an eddy covariance-based technique, ET was partitioned into its two components. Empirically nonlinear and linear models were used to investigate the observed fluxes and variables.

A low value of ET/ET_{eq} and SWC indicated a water deficit condition at this site. Drought conditions can reduce the surface conductance and hence the Priestley–Taylor

coefficient. T/ET was closely related to the plant growth stage under good water conditions. During drought conditions, the reduction of E was greater than that of T, and thus T/ET could increase.

The ecosystem photosynthesis parameters and Q_{10} for the growing season in the drought year 2015 were clearly different from those in the other three years, when F_{max} was much higher and Q_{10} was much lower. This difference also existed for dry conditions compared with wet conditions. The daily and monthly average Re values were positively and linearly correlated with GPP.

With multiple stepwise linear regression, the water and carbon fluxes can be explained by different values and types of variables on different timescales. For ET and E, SWC was the most important predictor, whereas EVI was the main predictor for T. For the carbon dioxide flux, EVI was the most important variable in explaining the variability on different temporal scales, except for Re where SWC was most significant on the daily scale.

Data Availability

The data used to support the findings of the study can be obtained from the corresponding author upon request.

Conflicts of Interest

The authors declare that they have no conflicts of interest.

Acknowledgments

This research was funded by the Second Tibetan Plateau Scientific Expedition and Research (STEP) Program (Grant no. 2019QZKK0105) and the National Natural Science Foundation of China (Grant nos. 41905010 and 41975017).

References

[1] W. T. Jaksa, V. Sridhar, J. L. Huntington, and M. Khanal, "Evaluation of the complementary relationship using Noah land surface model and north American regional reanalysis (NARR) data to estimate evapotranspiration in semiarid ecosystems," *Journal of Hydrometeorology*, vol. 14, no. 1, pp. 345–359, 2013.

[2] M. Jung, M. Reichstein, P. Ciais et al., "Recent decline in the global land evapotranspiration trend due to limited moisture supply," *Nature*, vol. 467, no. 7318, pp. 951–954, 2010.

[3] Z. Hu, G. Yu, Y. Fu et al., "Effects of vegetation control on ecosystem water use efficiency within and among four grassland ecosystems in China," *Global Change Biology*, vol. 14, no. 7, pp. 1609–1619, 2008.

[4] S. P. Good, D. Noone, and G. Bowen, "Hydrologic connectivity constrains partitioning of global terrestrial water fluxes," *Science*, vol. 349, no. 6244, pp. 175–177, 2015.

[5] J. von Buttlar, J. Zscheischler, A. Rammig et al., "Impacts of droughts and extreme temperature events on gross primary production and ecosystem respiration: a systematic assessment across ecosystems and climate zones," *Biogeosciences Discussions*, vol. 15, pp. 1–39, 2017.

[6] B. L. Xue, L. Wang, X. Li, K. Yang, D. Chen, and L. Sun, "Evaluation of evapotranspiration estimates for two river basins on the Tibetan Plateau by a water balance method," *Journal of Hydrology*, vol. 492, pp. 290–297, 2013.

[7] G. Song, Y. Tang, and X. Cui, "Characterizing evapotranspiration over a meadow ecosystem on the Qinghai-Tibetan Plateau," *Journal of Geophysical Research Atmospheres*, vol. 113, pp. 693–702, 2008.

[8] L. Wang, H. Liu, Y. Shao, Y. Liu, and J. Sun, "Water and CO2 fluxes over semiarid alpine steppe and humid alpine meadow ecosystems on the Tibetan Plateau," *Theoretical & Applied Climatology*, vol. 131, no. 1-2, pp. 1–10, 2016b.

[9] N. Ma, Y. Zhang, Y. Guo, H. Gao, H. Zhang, and Y. Wang, "Environmental and biophysical controls on the evapotranspiration over the highest alpine steppe," *Journal of Hydrology*, vol. 529, pp. 980–992, 2015.

[10] B. Niu, Y. He, and X. Zhang, "CO2 exchange in an alpine swamp meadow on the central Tibetan plateau," *Wetlands*, vol. 37, pp. 525–543, 2017.

[11] M. Du, Y. Li, F. Zhang et al., "Characteristics and scenarios projection of NEE change in an alpine meadow on the Tibetan Plateau," *International Journal of Global Warming*, vol. 24, no. 3/4, p. 307, 2021.

[12] S. Gu, Y. Tang, X. Cui et al., "Energy exchange between the atmosphere and a meadow ecosystem on the Qinghai-Tibetan Plateau," *Agricultural and Forest Meteorology*, vol. 129, no. 3-4, pp. 175–185, 2005.

[13] P. Mason, "Atmospheric boundary layer flows: their structure and measurement," *Boundary-Layer Meteorology*, vol. 72, no. 1-2, pp. 213-214, 1995.

[14] C. J. Moore, "Frequency response corrections for eddy correlation systems," *Boundary-Layer Meteorology*, vol. 37, no. 1-2, pp. 17–35, 1986.

[15] E. K. Webb, G. I. Pearman, and R. Leuning, "Correction of flux measurements for density effects due to heat and water vapour transfer," *Quarterly Journal of the Royal Meteorological Society*, vol. 106, no. 447, pp. 85–100, 1980.

[16] T. Foken and B. Wichura, "Tools for quality assessment of surface-based flux measurements," *Agricultural and Forest Meteorology*, vol. 78, no. 1-2, pp. 83–105, 1996.

[17] T. M. Scanlon and P. Sahu, "On the correlation structure of water vapor and carbon dioxide in the atmospheric surface layer: a basis for flux partitioning," *Water Resources Research*, vol. 44, no. 10, Article ID W10418, 2008.

[18] L. M. I. Aires, C. A. Pio, and J. S. Pereira, "Carbon dioxide exchange above a mediterranean C3/C4 grassland during two climatologically contrasting years," *Global Change Biology*, vol. 14, no. 3, pp. 539–555, 2008.

[19] Y. Igarashi, T. O. Kumagai, N. Yoshifuji et al., "Environmental control of canopy stomatal conductance in a tropical deciduous forest in northern Thailand," *Agricultural and Forest Meteorology*, vol. 202, pp. 1–10, 2015.

[20] J. L. Monteith and M. H. Unsworth, "Principles of environmental physics: plants, animals, and the atmosphere," 2013.

[21] F. Zhang, H. Li, and W. Wang, "Net radiation rather than surface moisture limits evapotranspiration over a humid alpine meadow on the northeastern Qinghai-Tibetan Plateau," *Ecohydrology*, vol. 11, no. 2, 2017.

[22] Z. Hu, S. Li, G. Yu et al., "Modeling evapotranspiration by combing a two-source model, a leaf stomatal model, and a light-use efficiency model," *Journal of Hydrology*, vol. 501, pp. 186–192, 2013.

[23] G. Zhu, Y. Su, X. Li, K. Zhang, and C. Li, "Estimating actual evapotranspiration from an alpine grassland on Qinghai-Tibetan plateau using a two-source model and parameter

uncertainty analysis by Bayesian approach," *Journal of Hydrology*, vol. 476, pp. 42–51, 2013.

[24] N. Raz-Yaseef, D. Yakir, G. Schiller, and S. Cohen, "Dynamics of evapotranspiration partitioning in a semi-arid forest as affected by temporal rainfall patterns," *Agricultural and Forest Meteorology*, vol. 157, pp. 77–85, 2012.

[25] R. L. Scott and J. A. Biederman, "Partitioning evapotranspiration using long-term carbon dioxide and water vapor fluxes," *Geophysical Research Letters*, vol. 44, no. 13, pp. 6833–6840, 2017.

[26] L. Shang, Y. Zhang, S. Lü, and S. Wang, "Energy exchange of an alpine grassland on the eastern Qinghai-Tibetan Plateau," *Science Bulletin*, vol. 60, no. 4, pp. 435–446, 2015.

[27] P. Krishnan, T. P. Meyers, R. L. Scott, L. Kennedy, and M. Heuer, "Energy exchange and evapotranspiration over two temperate semi-arid grasslands in North America," *Agricultural and Forest Meteorology*, vol. 153, pp. 31–44, 2012.

[28] C. P. Ghimire, M. W. Lubczynski, L. A. Bruijnzeel, and D. Chavarro-Rincón, "Transpiration and canopy conductance of two contrasting forest types in the lesser Himalaya of central Nepal," *Agricultural and Forest Meteorology*, vol. 197, pp. 76–90, 2014.

[29] Z. Gaofeng, L. Ling, S. Yonghong et al., "Energy flux partitioning and evapotranspiration in a sub-alpine spruce forest ecosystem," *Hydrological Processes*, vol. 28, no. 19, pp. 5093–5104, 2014.

[30] W. Zhao, B. Liu, X. Chang et al., "Evapotranspiration partitioning, stomatal conductance, and components of the water balance: a special case of a desert ecosystem in China," *Journal of Hydrology*, vol. 538, pp. 374–386, 2016.

[31] L. Wang, H. Liu, and C. Bernhofer, "Grazing intensity effects on the partitioning of evapotranspiration in the semiarid typical steppe ecosystems in Inner Mongolia," *International Journal of Climatology*, vol. 36, no. 12, pp. 4130–4140, 2016a.

[32] Y. Ryu, D. D. Baldocchi, S. Ma, and T. Hehn, "Interannual variability of evapotranspiration and energy exchange over an annual grassland in California," *Journal of Geophysical Research*, vol. 113, no. D9, Article ID D09104, 2008.

[33] D. D. Baldocchi and L. Xu, "What limits evaporation from Mediterranean oak woodlands – the supply of moisture in the soil, physiological control by plants or the demand by the atmosphere?" *Advances in Water Resources*, vol. 30, no. 10, pp. 2113–2122, 2007.

[34] K. G. Mcnaughton and T. W. Spriggs, "A mixed-layer model for regional evaporation," *Boundary Layer Meteorology*, vol. 34, no. 3, pp. 243–262, 1986.

[35] G. Song, Y. Tang, and X. Cui, "Charaterizing evapotranspiration over a meadow ecosystem on the Qinghai-Tibetan Plateau," *Journal of Geophysical Research Atmospheres*, vol. 113, no. D8, 2008.

[36] E. Falge, D. Baldocchi, R. Olson et al., "Gap filling strategies for defensible annual sums of net ecosystem exchange," *Agricultural and Forest Meteorology*, vol. 107, no. 1, pp. 43–69, 2001.

[37] B. Wang, H. Jin, Q. Li et al., "Diurnal and seasonal variations in the net ecosystem CO2 exchange of a pasture in the three-river source region of the Qinghai-Tibetan Plateau," *PLoS One*, vol. 12, no. 1, Article ID e0170963, 2017.